

Heterogeneous plastic deformation in bimodal bulk ultrafine-grained nickel

Quang Hien Bui

Received: 5 July 2011 / Accepted: 19 September 2011 / Published online: 1 October 2011
© Springer Science+Business Media, LLC 2011

Abstract Heterogeneous plastic deformation behavior of two bimodal ultrafine-grained nickel materials with different ultrafine-grained (UFG) and coarse-grained (CG) components fractions was investigated experimentally at the grain level. The prismatic specimens were deformed quasistatically up to 10% axial plastic strain using compression test at room temperature. The local microstructure of the initial and deformed samples was measured by electron backscattered diffraction pattern analysis in a scanning electron microscope. It was found that the plastic deformation of bimodal materials is highly heterogeneous and the degree of heterogeneity depends strongly on the grain size distribution and the volume fraction of the CG component. The large localized plastic strain within the coarse grains was observed during compression. The strain localization resulted in occurrence of debonding and cracks in the UFG region or in the interface between CG and UFG components.

Introduction

Bulk nanocrystalline (NC) and ultrafine-grained (UFG) materials, with average grain size typically below 1 μm , have usually very high strength in comparison to their conventional coarse-grained (CG) counterparts. However,

it was observed that as the strength increases with grain refinement, most materials exhibit low ductility, which limits their structural application [1–3]. Therefore, it is imperative to improve ductility of NC/UFG materials for their structural applications which often require both high strength and good ductility [4]. It has been suggested that, one strategy to enhance the ductility of NC/UFG materials is to process a bimodal grain structure, in which the fine grains provide strength, and the coarse grains improve ductility [5–13]. Wang et al. [5] proposed a thermomechanical treatment of NC Cu that result in a bimodal grain size distribution, with micrometer-sized grains embedded inside a matrix of NC grains. This special material exhibited a high tensile ductility and retained relatively high strength. Lavernia and co-workers [6, 7, 14, 15] proposed a processing of cryomilled aluminum alloys with a bimodal microstructure which was successfully performed via consolidation of a mixture of nanostructured powders with unmilled coarse-grained powders to achieve an excellent combination of strength and ductility. High strength and good ductility were obtained in the nanostructured Ni [8, 9, 12] and Fe [11, 16] with a broad grain size or a bimodal grain size distribution. The knowledge of deformation mechanism of each component in bulk bimodal microstructure is useful for the concept of this kind of materials. However, few studies were devoted to the mechanism of deformation of this kind of material [8, 15] and these studies did not show completely the different deformation mechanism of its two CG and UFG components.

In the study of Fan et al. [15], the deformation and fracture mechanisms during compression and tension tests of bimodal microstructures consisting of coarse grains evenly distributed in the UFG matrices which have various average grain sizes were discussed. The authors found that

Q. H. Bui (✉)
LPMTM-CNRS, Institut Galilée, Université Paris 13,
99 Avenue J.B. Clement, 93430 Villetaneuse, France
e-mail: buiquanghien@gmail.com

Present Address:

Q. H. Bui
Aluminium Research Centre—REGAL, Laval University,
Quebec G1V0A6, Canada

the plastic deformation of the UFG Al–Mg alloys with a bimodal structure was highly localized. They mentioned also that the fracture of the alloys was attributed to shear localization under the compression tests and to a combination of shear localization, cavitation, and necking under tensile tests. Shen et al. [8] used the strain rate sensitivity and flow stress activation volume to interpret the deformation mechanism controlled in NC Ni with broad grain size distribution.

In the study of Lee et al. [14], the microstructure, mechanical properties, and deformation response of bimodal structure Al–7.5Mg were investigated. The authors proved that the observations of Vickers and Brinell indentations on bimodal materials with different volume fractions of CG could be used to evaluate their plastic deformation response. They also remarked that the bimodal grain structures exhibit unusual deformation mechanisms similar to the ductile-phase toughening of brittle materials, however, further experiments must be directed at understanding these deformation mechanisms and the patterns of strain distribution within the microstructure.

In the present study, an experimental program was carried out to investigate the deformation mechanisms and microstructural evolution of both phases (CG and UFG) components of bulk bimodal Ni during plastic deformation. By using the electron back scatter diffraction (EBSD) technique and scanning electron microscope (SEM), the microstructure evolution was examined on the same area before and after compression up to plastic strain around 10%. By dividing the grain size distribution obtained by an orientation imaging microscopy software into two parts containing the CG and UFG components, the microstructural evolution of these two components was characterized individually.

Experimental procedures

Bulk bimodal materials were consolidated from blends of high purity ($\sim 99.99\%$) Ni nanopowder (NP) with a conventional coarse-grained powder (CP). The NP powder was supplied by Argonide Corporation (Sanford, FL) and synthesized by electro-explosion of wires [17, 18]. The NP powder having spherical particles with nominal size of about 100 nm, as shown by former transmission electron microscopy (TEM) investigations [13, 19], was used. In the initial NP powder, the relative frequency of twin boundaries among the (1 1 1) lattice planes was about 2–3%, as determined from the twin-spacings in TEM images. The particles in the CP powder (produced by Goodfellow) were agglomerated into particle clusters of about 50 μm in diameter as it is revealed by the scanning electron microscopy (SEM) [13]. The average size of the individual particles within the clusters was about 5 μm .

Two specimens with different volume fractions of NP and CP powders were prepared. Sample A was processed by mixing ~ 33 vol.% CP and ~ 67 vol.% NP powders while for sample B the relative amount of the CP powder was only ~ 17 vol.%. The powders including the blends were handled and prepared in a glove box under inert gas (Ar) flow to minimize possible contamination. To reach an optimum distribution of the CP particles within the NP powder, the powders were mixed in a three-dimensional shaker mixer (Turbula[®] model T2F) for 6 h at RT. The different powders/blends were filled into stainless steel cans and degassed at room temperature (RT) for 1 week before consolidation using hot isostatic pressing (HIP).

The HIP procedure has been described in our previous articles [20–22]. The processing conditions were optimized to reach the desired microstructure having small porosity. The pressure and the temperature of the HIP cycles were set around 150 MPa and 700 °C, respectively. The duration of the HIP cycles was about 155 and 60 min for samples A and B, respectively. The pressure and the temperature were applied concomitantly. Both the heating and cooling rates were equal to 375 K/h.

Prismatic samples with dimensions of $3 \times 3 \times 5$ mm³ were cut from the sintered materials for mechanical tests. An Instron universal testing machine (model 1195) was used for the uniaxial compressive tests at RT and at the strain rate of 1.6×10^{-4} s⁻¹. The microstructure of the samples before and after deformation was characterized by TEM, SEM, and EBSD techniques. A JEOL-2011 electron microscope operating at 200 kV was used for TEM investigations. Thin foils for TEM were prepared using a Gatan precision ion polishing system (PIPS), with a current of 0.5 mA and a voltage of 5 kV at starting angles of $\pm 7^\circ$. The EBSD experiments were carried out on a Leo S340 SEM. Before EBSD analysis, samples were electropolished with A2 electropolishing solution from Struers at a voltage of 12 V for 15 s. The analyses were carried out using a step size of 200 nm. The grain size distribution, the texture, and the grain boundary misorientation distribution were determined using an orientation imaging microscopy (OIM) software from TSL.

Results and discussions

Initial microstructure

The measurement of mass density of the consolidated samples was performed in accordance with Archimedes' principles using distilled water as the immersion medium at RT. The relative densities are 97 and 94% for the samples A and B, respectively. Figure 1 shows the surfaces of both bimodal materials observed by SEM. The area fraction was

Fig. 1 SEM images showing the cross section of the HIPed bimodal A (a) and bimodal B (b)

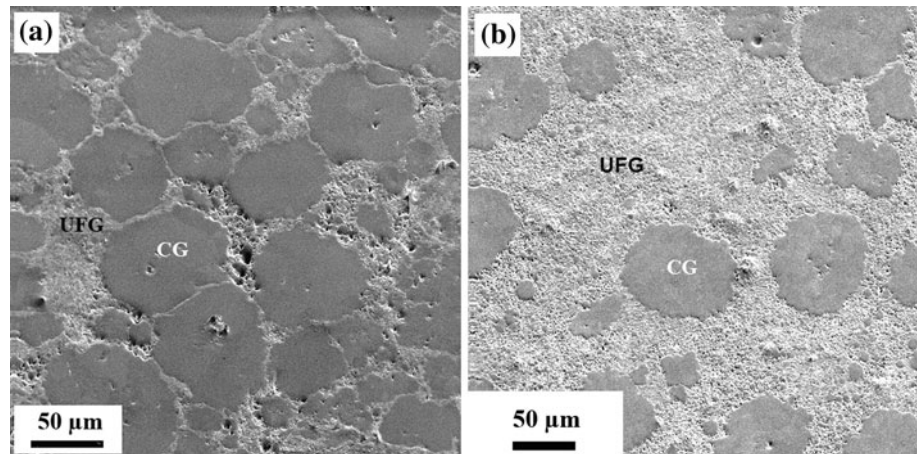


Fig. 2 EBSD images taken on surface of (a) bimodal A and (b) bimodal B samples

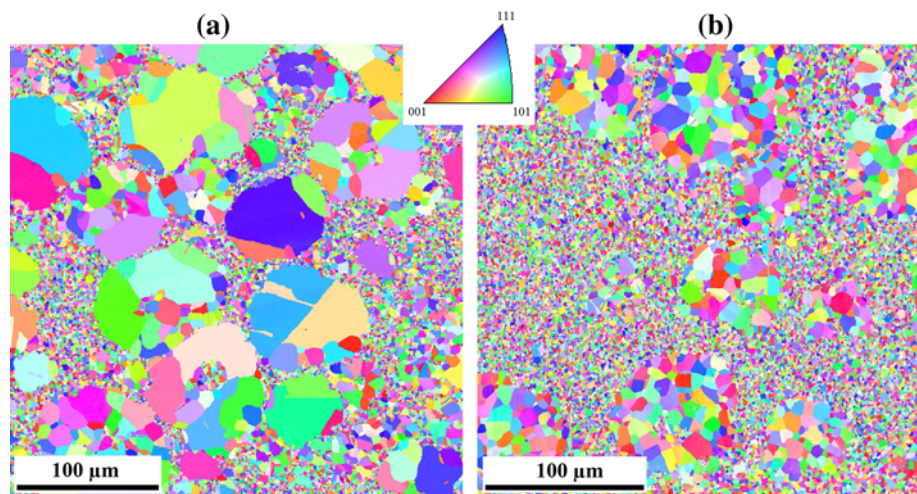
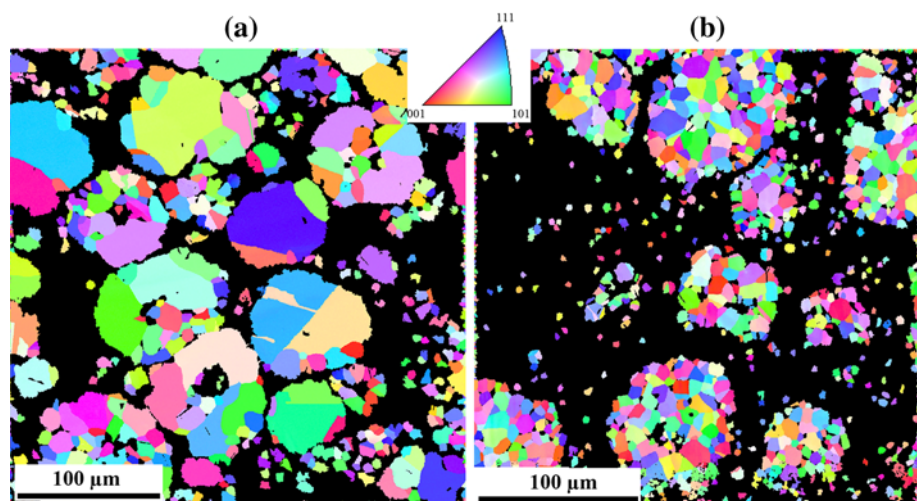


Fig. 3 EBSD images of CG phase taken on surface of (a) bimodal A and (b) bimodal B samples



determined by the IMAGE TOOL. The CG regions correspond to the gray regions, which occur approximately 61% of total surface for the bimodal A (Fig. 1a) and 39% for the bimodal B (Fig. 1b). Each CG region shows the spherical shape. The mean diameter of the CG region in the

both bimodal materials is the same and equal to about 50 μm. For both samples, the CG fraction evaluated from SEM data is higher than the volume fraction of the CP component in the powder blends measured before consolidation (see “[Experimental procedures](#)” section). This

Fig. 4 Grain size distribution of the coarse-grained phase determined in the bulk bimodal A (a) and bimodal B (b) materials using EBSD technique

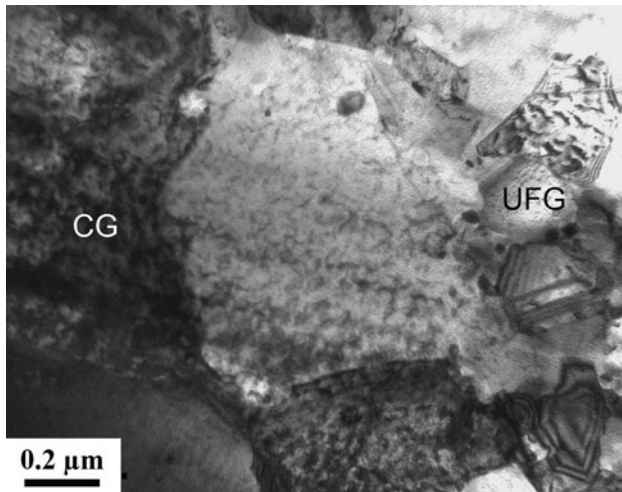
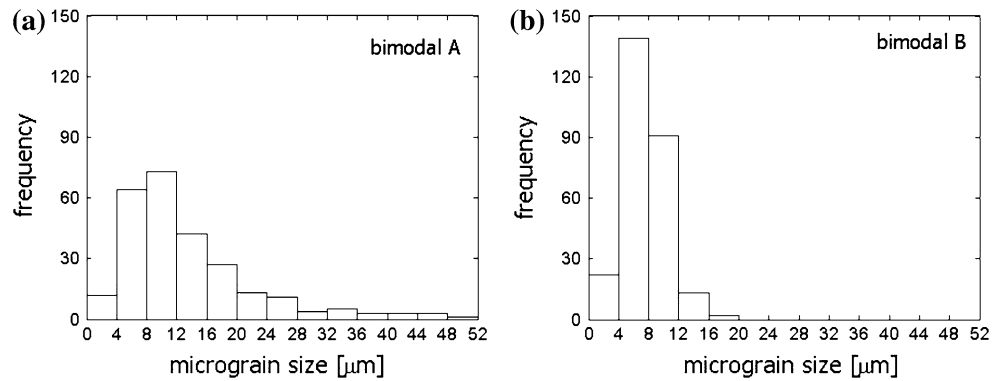


Fig. 5 TEM observation of the bulk bimodal A materials

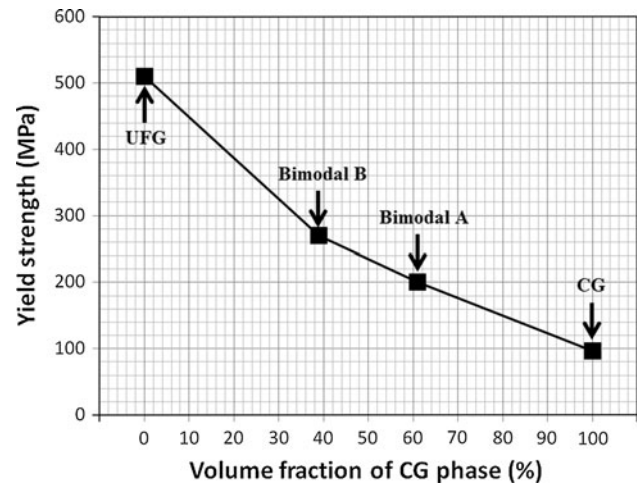


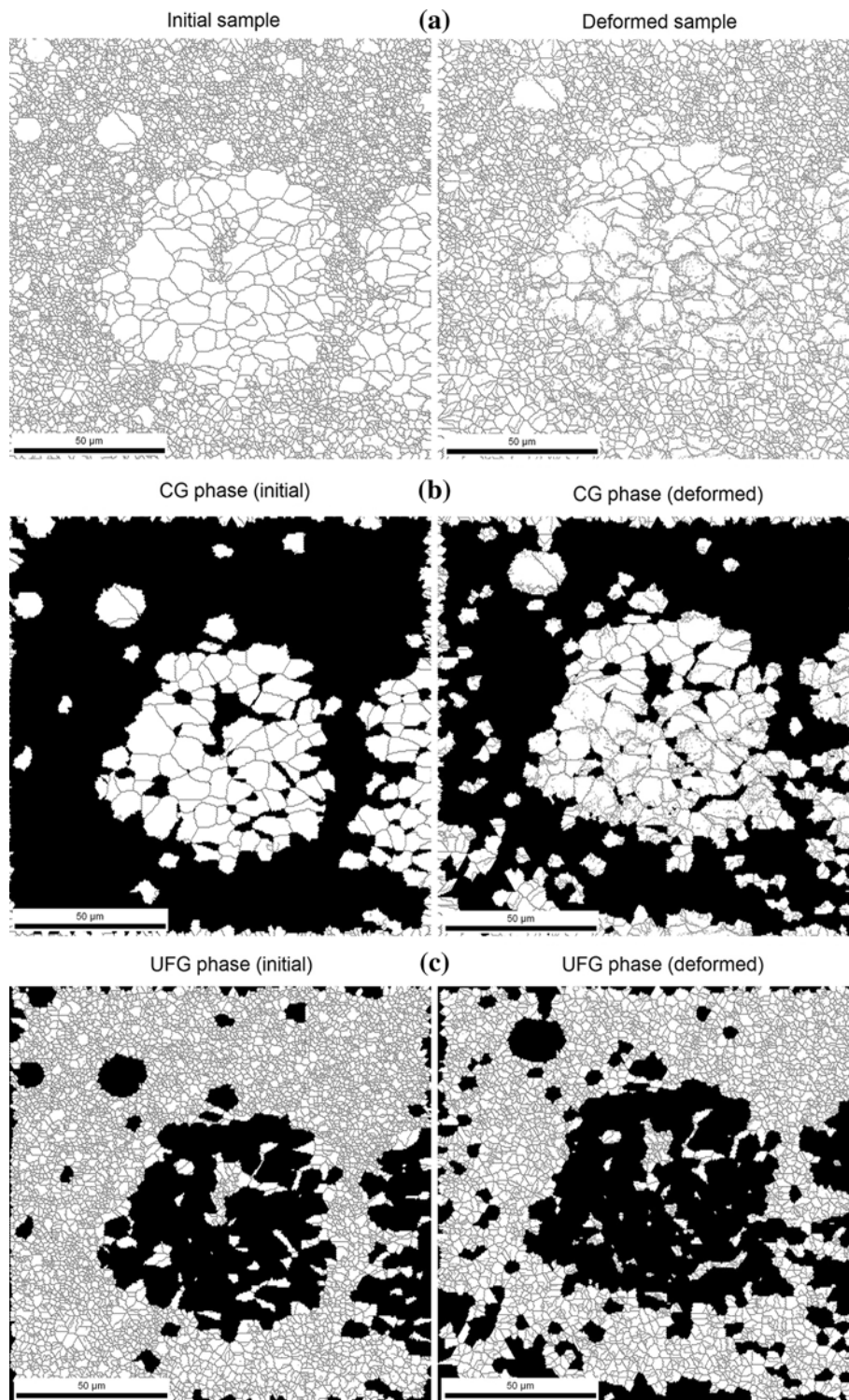
Fig. 6 Experimental yield strength as a function of volume fraction of CG phase

difference can be explained by the more dense powder microstructure in the CP powder compared to NP powder component. The dense particle packing in the CP powder is supported by the agglomeration of the particles as before mentioned.

Figure 2a, b shows the microstructure observed by EBSD technique for bimodal materials A and B, respectively. As expected from HIP-processing [2, 20], the microstructures obtained here exhibit a random crystallographic texture. In order to individually characterize the microstructure of CG and UFG phases, the partition option integrated in the OIM software was used. Figure 3 shows only the microstructure of the CG regions (with grain size higher than 5 μm) of the two bimodal materials. The black color regions show the UFG phase. It can be observed that the clusters of micrograins (coarse-grains) were regularly distributed in the UFG matrix. The mean grain size of micrograins located inside the CG clusters is 13 and 7 μm for samples A and B, respectively. Figure 4a, b shows the grain size distribution of the CG phase of the bulk for bimodal materials A and B, respectively. Dirras et al. [13]

mentioned that in the fully CG sample, the grain size (50–100 μm) is close or even larger than the agglomerate size in the initial CG powder. This indicates a grain-coalescence inside the CG agglomerates during HIP, which may also spread into the neighboring agglomerates. In the composite samples it seems that the UFG component acts against the coalescence of CG grains as the higher the UFG content, the lower the level of grain-growth in the CG component. Most probably, during powder mixing, NP particles got in between CG agglomerates which formed thin intergranular UFG domains between CG grains in the consolidated samples. The higher oxide content in this UFG component hinders the grain-boundary motion of CG grains during sintering, consequently reducing the grain-coalescence. This can be called as a “barrier effect” of UFG fraction on CG grains. Nevertheless, the lower degree of grain-coalescence in CG component of sample B can be partially attributed to the lower temperature and shorter time of sintering. It is noted that thermodynamic consideration suggests that coarser grains should grow at the expense of UFG grains during sintering of powder blends because of the higher

Fig. 7 (a) EBSD boundary maps of bimodal B sample before and after compression up to plastic strain of about 10%; (b) EBSD boundary maps of the CG phase extracted from (a); (c) EBSD boundary maps of the UFG phase extracted from (a)



specific grain-boundary area of the smaller grains. Consequently, if the UFG fraction had been oxide-free, its addition to the CG component most probably would have accelerated the grain coarsening during sintering.

Figure 5 shows the TEM microstructure of bimodal A materials. The grain size obtained by TEM experiments

indicates that the UFG grains phase has a log-normal size distribution with an average grain size about 400 nm in samples A and B. It must be noted that the same value of average grain size was found in the fully UFG specimen [13, 22]. The average grain sizes determined by OIM for UFG phase in bimodal A and B materials are about

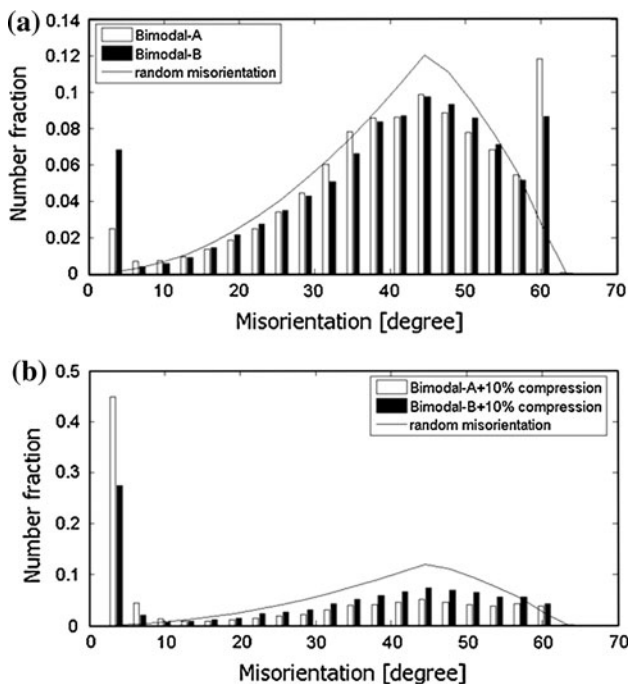


Fig. 8 Distributions of misorientation angles across the boundaries for bimodal materials A and B: (a) initial samples and (b) deformed samples

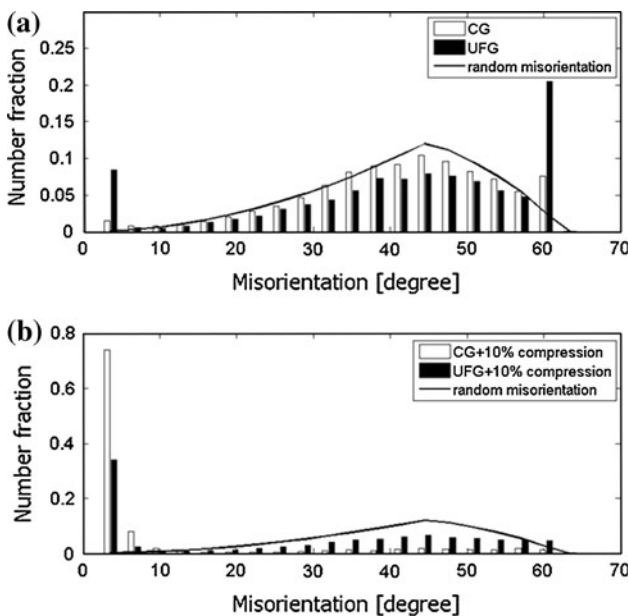


Fig. 9 Distributions of misorientation angles across the boundaries for CG and UFG components of bimodal A materials: (a) initial samples and (b) deformed samples

700 nm. These values are about 1.75 times larger than those determined by TEM, as in the EBSD scan the grains that are smaller than the step size (200 nm) have not been counted.

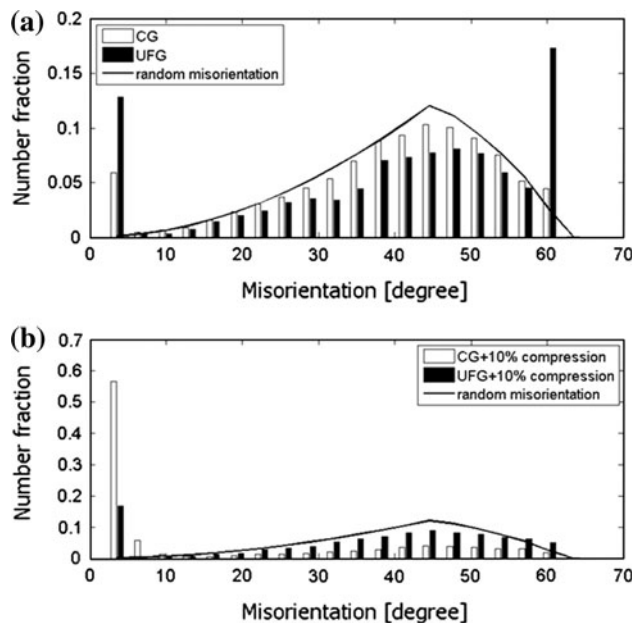


Fig. 10 Distributions of misorientation angles across the boundaries for CG and UFG components of bimodal B materials: (a) initial samples and (b) deformed samples

Deformed microstructure

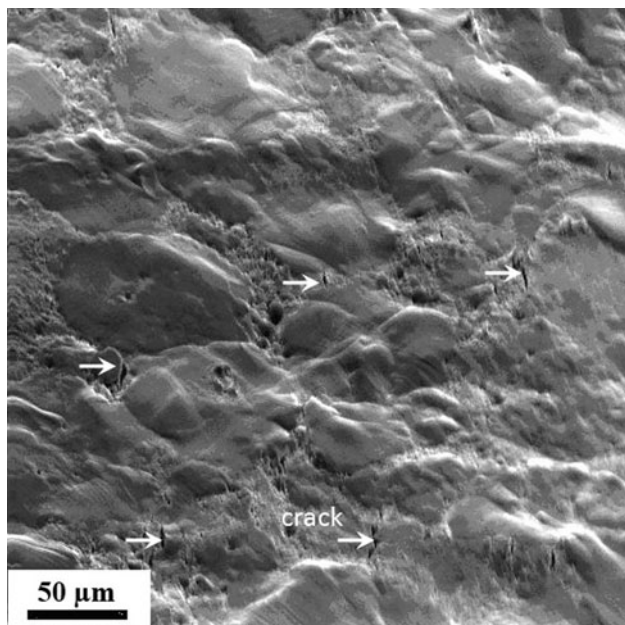
The yield strength obtained from compression tests was plotted as a function of the CG volume fraction in Fig. 6. The yield strength data of the unimodal materials, i.e., UFG and CG materials, was taken from Ref. [22]. It can be seen that the yield strength increases with decreasing the amount of the CG content of the samples. For example, the yield strength of bimodal B (≈ 270 MPa) is about 26% higher than that of bimodal A (≈ 200 MPa), but about half of the yield strength for the UFG counterpart.

Figure 7a shows the changes in the grain-boundary structure during plastic deformation of the bimodal B sample. Figure 7b and c shows the EBSD boundary maps of the CG and UFG phases, which were extracted from Fig. 7a. In this figure, the red and black lines represent the low angle grain boundaries (LAGBs) having misorientations between 2° and 15° and the high angle grain boundaries (HAGBs) with larger misorientations, respectively.

Figure 8a and b shows the distributions of misorientation angles across the boundaries for two bimodal materials at initial and deformed states, respectively. Figures 9 and 10 show the evolution of misorientation angles distributions during compression of the CG and UFG components of the bimodal materials A and B, respectively. A peak appears at approximately 60° in the misorientation distribution indicates the presence of $\Sigma 3$ boundaries such as coherent twin boundaries (TBs). The LAGBs and HAGBs fractions of two bimodal materials and their components at

Table 1 Evolution of LAGBs and HAGBs fraction of two bimodal materials and their components at initial and deformed state

	LAGBs ($\Delta\theta < 15^\circ$)		HAGBs ($\Delta\theta \geq 15^\circ$)	
	Initial sample (%)	Deformed sample (%)	Initial sample (%)	Deformed sample (%)
Bimodal A	5	51	95	49
CG (Bimodal A)	4	84	96	16
UFG (Bimodal A)	10	38	90	62
Bimodal B	8	31	92	69
CG (Bimodal B)	7	64	93	36
UFG (Bimodal B)	14	18	86	82

**Fig. 11** SEM images showing the lateral surface of the HIPed bimodal A samples after compression test at plastic strain of 10%

initial and deformed states are shown in Table 1. The experimental results show that:

- In both initial bimodal samples, the majority of the boundaries (95 and 92% for samples A and B, respectively) are high angle grain boundaries.
- After deformation up to 10% plastic strain, a tremendous increase of LAGBs is observed within the CG component most probably as a result of clustering of dislocations. The majority of LAGBs are formed in the vicinity of HAGBs (see the deformed state shown in Fig. 7b) as the latter boundaries act as obstacles to dislocations. A large fraction of LAGBs is also observed at the UFG/CG interfaces.
- In both initial bimodal materials, the coherent twin boundaries are found mainly in UFG component.
- At the same time, the twin boundary fraction decreased during plastic deformation that is a consequence of the interaction between TBs and dislocations, as reported

in some previous studies [21, 23]. The LAGBs formation and decrease of the TBs fraction indicate that the plastic deformation is basically controlled by dislocations at RT.

- The LAGBs observed in the bimodal A material increase from 5% (in the initial state) to 51% (in the deformed state), however, the LAGBs observed in the bimodal B increase from 8% (in the initial state) to 31% (in the deformed state). It means that formation of LAGBs in bimodal material during plastic deformation depends strongly not only on the grain size but also on the volume fraction of UFG or CG components. When grain size is large and volume fraction of UFG component is small, the LAGBs form significantly during plastic deformation.
- The formation of LAGBs observed in the CG component of bimodal materials A and B increases from 4% (initial state) to 84% (deformed state), and from 7% (initial state) to 64% (deformed state), respectively. However, the formation of LAGBs observed in the UFG component of two materials increases from 10% (initial state) to 38% (deformed state), and from 14% (initial state) to 18% (deformed state), respectively. These results confirmed that the increase of LAGBs is observed mostly within the CG component and a slight increase of LAGBs is observed in UFG component.
- EBSD map shows inhomogeneous strain between the UFG and CG regions after plastic deformation; and the strain was localized mainly in the CG regions. The strain inhomogeneity between two regions and the strain localization in CG regions were also observed by optical micrographs and corresponding digital image correlation technique for bimodal Al–Mg alloy [24].

The lateral surfaces after the compression test were examined using SEM. Figure 11 showed a typical lateral surface of sample bimodal A deformed at about 10% plastic strain. It can be remarked that: (i) The CG regions deforms differently than UFG regions; (ii) Slip bands are found inside of coarse grain; (iii) Several cracks (debonding) are found in the UFG region or in the interface between

UFG and CG regions; (iv) Based on the morphology changes of CG grains in bimodal A (by analyzing Figs. 1a and 11 and by comparing these two figures), the mean computed strain for these grains is about 29% which is about twice the imposed macroscopic plastic strain (10%) similarly as reported previously on coarse Al grains embedded in UFG Al matrix [20]. The larger strain of the CG grains and the smaller strain of UFG grains may be a result of strain localization during compression. The strain may be localized in a cross-section of the sample where the area fraction of soft CG component is larger than the average. The strain localization results in a possibility of occurrence of debonding and cracks in the UFG region or in the interface between UFG and CG regions.

Conclusion

The bulk bimodal nickel specimens with a random crystallographic texture were consolidated by hot isostatic pressing of blends of NC and conventional microcrystalline powders with controlled volume fractions. The microstructure evolution were examined on the same area of lateral surface of initial and deformed samples using the EBSD analysis and SEM technique. It was found that:

- The plastic deformation of bimodal materials is highly heterogeneous and the degree of heterogeneity depends strongly on the grain size distribution and the volume fraction of the CG component.
- The microstructure evolution of different components of bimodal materials revolves differently.
- The larger strain of the coarse grains and the smaller strain of ultrafine grains may be a result of strain localization during compression of bimodal material.
- The strain localization results in a possibility of occurrence of debonding and cracks in the UFG region or in the interface between UFG and CG regions.

Acknowledgements The author is very grateful to J.-P. Michel for HIPing operations.

References

1. Dalla Torre F, Van Swygenhoven H, Victoria M (2002) *Acta Mater* 50:3957
2. Cao W, Dirras G, Benyoucef M, Bacroix B (2007) *Mater Sci Eng A* 462:100
3. Bui QH, Dirras G, Ramtani S, Gubicza J (2010) *Mater Sci Eng A* 32:1612
4. Wang YM, Ma E (2004) *Acta Mater* 52:1699
5. Wang Y, Chen M, Zhou F, Ma E (2002) *Nature* 419:912
6. Witkin D, Lee Z, Rodriguez R, Nutt S, Lavernia E (2003) *Scripta Mater* 49:297
7. Han BQ, Lee Z, Witkin D, Nutt S, Lavernia EJ (2005) *Metall Mater Trans A* 36:957
8. Shen X, Lian J, Jiang Z, Jiang Q (2008) *Mater Sci Eng A* 487:410
9. Zhao Y, Topping T, Bingert JF, Thornton JJ, Dangelewicz AM, Li Y, Liu W, Zhu Y, Zhou Y, Lavernia EJ (2008) *Adv Mater* 20:3028
10. Xia S, Vychigzhanina L, Wang J, Alexandrov I, Sharafutdinov A (2008) *Mater Sci Eng A* 490:471
11. Srinivasarao B, Oh-ishi K, Ohkubo T, Mukai T, Hono K (2008) *Scripta Mater* 58:759
12. Prasad M, Suwas S, Chokshi A (2009) *Mater Sci Eng A* 503:86
13. Dirras G, Gubicza J, Ramtani S, Bui QH, Szilagy T (2010) *Mater Sci Eng A* 527:1206
14. Lee Z, Witkin D, Radmilovic V, Lavernia E, Nutt S (2005) *Mater Sci Eng A* 410–411:462
15. Fan G, Choo H, Liaw P, Lavernia E (2006) *Acta Mater* 54:1759
16. Srinivasarao B, Oh-ishi K, Ohkubo T, Hono K (2009) *Acta Mater* 57:3277
17. Tepper F (1998) *Met Powder Rep* 53:31
18. Kwon Y, Jung Y, Yavorovsky NA, Illyin AP, Kim J (2001) *Scripta Mater* 44:2247
19. Bui QH (2010) *Polycristaux a grains fins elaborés par metallurgie des poudres : microstructures, propriétés mécaniques (in french)*. Editions universitaires europeenne, ISBN :978-613-1-51805-8
20. Billard S, Fondere J, Bacroix B, Dirras G (2006) *Acta Mater* 54:411
21. Gubicza J, Bui QH, Fellah F, Dirras G (2009) *J Mater Res* 24:217
22. Bui QH, Pham XT (2011) *Int J Mech Sci* 53:812
23. Gubicza J, Bui QH, Fellah F, Szasz N, Dirras G (2008) *Mater Sci Forum* 589:93
24. Ahn B, Lavernia EJ, Nutt SR (2008) *J Mater Sci* 43:7403. doi: [10.1007/s10853-008-2950-1](https://doi.org/10.1007/s10853-008-2950-1)